International Symposium
On Turbulence and Shear Flow
Phenomena (TSFP-9)
June 30 - July 3, 2015 Melbourne, Australia

LARGE-EDDY SIMULATION OF SPRAY COMBUTION IN A SECTOR COMBUSTOR FOR REGIONAL JET AIRCRAFT ENGINE - EFFECT OF DOUBLE-WALL LINER ON NOx FORMATION -

Hideki Moriai
Integrated Defense & Space Systems
Mitsubishi Heavy Industries, Ltd.
1200, Higashi Tanaka, Komaki, Aichi 485-8561, Japan
hideki_moriai@mhi.co.jp

Kotaro Hori
Numerical Flow Designing, Co., Ltd.
1-10-10, Higashi-Gotanda, Shinagawa-ku, Tokyo 141-0022, Japan
hori@nufd.jp

Ryoichi Kurose, Satoru Komori
Department of Mechanical Engineering and Science
Kyoto Univbersity
Kyoto daigaku-Katsura, Nishikyo-ku, Kyoto 615-8540, Japan
kurose@mech.kyoto-u.ac.jp, komori@mech.kyoto-u.ac.jp

ABSTRACT

Large-eddy simulation (LES) is applied to a turbulent spray combustion field in a sector combustor for a regional jet aircraft engine under development, and the effects of liner-cooling air flow outlet location (i.e., effect of single/double wall liners) on the combustion behaviour and NOx emission are investigated. The combustor is designed based on RQL (Rich burn, Quick quench, Lean burn) concept to reduce NOx emission. In the LES, Jet-A1 is used as liquid fuel, and individual droplet motion is tracked in a Lagrangian manner with a parcel model. As the turbulent combustion model, an extended flamelet/progress-variable approach, in which heat transfer between droplets and ambient gas including radiation and heat loss from walls can be taken into account, is employed. A detailed chemistry mechanism of Jet-A1 with 1537 reactions and 274 chemical species is used. The radiative heat transfer is computed by the discrete ordinate (DO) method. The LES results show general agreement with the experimental data, and the double wall liner design seems desirable for low NOx RQL combustor.

INTRODUCTION

Due to increasing environmental awareness worldwide, aircraft emission (NOx, CO, PM, etc.) control have become more stringent in recent years. The aircraft exhaust gas amount is severely limited by the regulations adopted by CAEP (Committee on Aviation Environmental Protection). By CAEP/6 regulations which came into effect in 2008, NOx emission is reduced by 12% and by CAEP/8 regulations which will come into effect in 2014 NOx will be reduced by further 15%. NOx regulation is expected to be more stringent in the future steadily (Moriai and Miyake, 2008).

With this background, the low NOx combustor technology is very important in the development of the latest aircraft engines. However, the precise predictions of emission from the combustor including combustion characteristics are so difficult that the development cycles including hardware design, fabricating and evaluation tests are generally repeated many times to meet specification requirements and end up with huge cost and time. Therefore, if many hardware tests are substituted with numerical simulations, significant development cost reduction is possible. Because the internal flow of the combustor is composed of complex phenomena, including spray atomization, turbulent mixing, and chemical reactions, numerical simulation is very difficult. In recent years, LES (Large-eddy simulation) that can simulate unsteady turbulent flow well attracts attention.

The purpose of this study is, therefore, to apply the LES to a turbulent spray combustion field in a sector combustor for a regional jet aircraft engine under development, and to predict the spray combustion behaviour and emissions such as NOx and soot. Special attentions are focused on the effect of liner-cooling air flow outlet location (i.e., effect of single/double wall liner designs) on the NOx emission.

NUMERICAL METHODS

Large-Eddy Simulation

In this work, the compressible reacting flow equations with two-way coupling between the continuous phase (gas phase) and dispersed phase (fuel droplets) were solved using an unstructured large-eddy simulation (LES) solver: FrontFlow/Red as extended by Kyoto University, CRIEPI and NuFD (Numerical Flow Designing, Co., Ltd.), referred to as FFR-Comb. The numerical methods used here are basically the same as those written in our previous paper (Morial et al., 2013), but the compressible scheme in Demirdžić et al. (1993) is newly employed (Tachibana et al., 2015). As turbulent combustion model, a flamelet/progress-variable approach which is originally

developed by Pierce & Moin (2004) is extended and employed by ourselves (Baba & Kurose, 2008, Fujita et al., 2013; Kitano et al., 2013).

The governing equations for the gas phase shown below are discretized in space using a second-order finite volume formation, using a first-order implicit Euler method for the time advancement:

$$\frac{\partial \bar{\rho}}{\partial t} + \nabla \cdot (\bar{\rho}\tilde{\boldsymbol{u}}) = S_m, \tag{1}$$

$$\frac{\partial \bar{\rho}\tilde{\boldsymbol{u}}}{\partial t} + \nabla \cdot (\bar{\rho}\tilde{\boldsymbol{u}}\tilde{\boldsymbol{u}}) = -\nabla \bar{p} + \nabla \cdot \bar{\boldsymbol{\sigma}} + \nabla \cdot \bar{\boldsymbol{\tau}} + S_{\boldsymbol{u}}, \tag{2}$$

$$\frac{\partial \bar{\rho}\tilde{Z}}{\partial t} + \nabla \cdot \left(\bar{\rho}\tilde{\boldsymbol{u}}\tilde{Z}\right) = \nabla \cdot \left(\bar{\rho}\widetilde{D_Z}\nabla\tilde{Z}\right) + \nabla \cdot \boldsymbol{q}_Z + S_Z, \tag{3}$$

$$\frac{\partial \bar{\rho}\tilde{C}}{\partial t} + \nabla \cdot \left(\bar{\rho}\tilde{\boldsymbol{u}}\tilde{C}\right) = \nabla \cdot \left(\bar{\rho}\widetilde{D_C}\nabla\tilde{C}\right) + \nabla \cdot \boldsymbol{q}_C + \widetilde{\dot{\omega}_C}, \tag{4}$$

$$\frac{\partial \bar{\rho}\tilde{h}}{\partial t} + \nabla \cdot \left(\bar{\rho}\tilde{\boldsymbol{u}}\tilde{h}\right) = \frac{D\bar{p}}{Dt} + \nabla \cdot \left(\bar{\rho}\widetilde{D_h}\nabla\tilde{h}\right) + \nabla \cdot \boldsymbol{q}_h + S_h, \tag{5}$$

where ρ is the density, $\boldsymbol{u}$ is the velocity vector, p is the pressure, $\boldsymbol{\sigma}$ is the stress tensor, Z is the mixture fraction, C is the progress variable defined as the summation of the product gases ($C = Y_{CO} + Y_{CO_2} + Y_{H_2} + Y_{H_2O}$) and h is the total enthalpy. D and $\boldsymbol{q}$ are the diffusion coefficient and subgrid-scale term, respectively, while $\boldsymbol{\tau}$ is the SGS stress term, and $\boldsymbol{q}_Z$, $\boldsymbol{q}_C$ and $\boldsymbol{q}_h$ are the SGS terms for scalars. $\dot{\omega}_C$ is the production rate for the progress variable, while $\bar{}$ and $\tilde{}$ denote LES filtering and Favre averaging, respectively.

The fuel droplets are modeled as evaporating in the high temperature region, following which the evaporated fuel gas reacts with oxygen. The fuel droplets are tracked individually in a Lagrangian manner, and a first-order implicit Euler method is used for the time advancement. The governing equations for droplet motion can be described as follows:

$$\frac{d\boldsymbol{x}_d}{dt} = \boldsymbol{u}_d, \tag{6}$$

$$\frac{d\boldsymbol{u}_d}{dt} = \frac{f_1}{\tau_d}(\tilde{\boldsymbol{u}} - \boldsymbol{u}_d), \tag{7}$$

$$\frac{dT_d}{dt} = \frac{\mathrm{Nu}}{3\mathrm{Pr}}\left(\frac{\bar{c}_p}{c_{p,d}}\right)\left(\frac{f_2}{\tau_d}\right)(\tilde{T} - T_d), \tag{8}$$

$$\frac{dm_d}{dt} = -\frac{\mathrm{Sh}}{3\mathrm{Sc}}\frac{m_d}{\tau_d}\ln(1 + B_M), \tag{9}$$

where $\boldsymbol{x}_d$ is the droplet location, $\boldsymbol{u}_d$ is the droplet velocity vector, T_d is the droplet temperature, m_d is the droplet mass, and τ_d is the droplet relaxation time. The terms c_p and $c_{p,d}$ are the specific heat of the gas and the droplet respectively, while f_1 and f_2 are correlation coefficients due to the droplet evaporation (Kurose et al., 2003; Nakamura et al., 2005). B_M is the mass transfer number for evaporation and Nu, Pr, Sh and Sc are the Nusselt, Prandtl, Sherwood and Schmidt numbers, respectively. The S term in Equations (1) to (3) and (5) denotes source terms due to interactions between the gas and droplet phases and is determined using the particle-source-in-cell (PSI-Cell) method as follows:

$$S_m = -\frac{1}{\Delta V}\sum_N \frac{dm_d}{dt}, \tag{10}$$

$$S_{\boldsymbol{u}} = -\frac{1}{\Delta V}\sum_N \frac{dm_d\boldsymbol{u}_d}{dt}, \tag{11}$$

$$S_Z = -\frac{1}{\Delta V}\sum_N \frac{dm_d}{dt}, \tag{12}$$

$$S_h = -\frac{1}{\Delta V}\sum_N \left[Q_d + \frac{dm_d}{dt}L_V\right], \tag{13}$$

where ΔV is the control volume, N is the number of droplets in the control volume and L_V is the latent heat. Here Q_d is the heat transferred by convection from the gas to liquid phase.

The flamelet calculations to generate the flamelet library for diffusion flame were carried out using FLAMEMASTER code (Pitsch, 1998). Strictly speaking, the mixture fraction Z, which should be a conserved scalar in flamelet models, is no longer a conserved scalar in the gas phase (Watanabe et al., 2007; Baba and Kurose, 2008; Luo et al., 2013). However, since this Z-transfer effect is very difficult to incorporate when generating the flamelet library, it was neglected and a flamelet library for pure gaseous combustion was used in the present LES. As liquid fuel, jet-A1 which is treated as a mixture composed of dodecane ($C_{12}H_{26}$), iso-octane (C_8H_{18}) and toluene (C_7H_8) with mass fractions of 0.45, 0.29 and 0.26, respectively, is used and the chemical mechanism including 1537 reactions among 274 chemical species is employed (Blanquart et al., 2009; Narayanaswamy et al., 2010; Watanabe et al., 2014). Concerning the vaporization of droplets, a non-equilibrium Langmuir-Knudsen evaporation model is used (Miller and Bellan, 1999; Kitano et al., 2014a, 2014b). The initial droplet size distribution of the injected fuel droplets is given according to the experimental data (Moriai et al., 2011). The radiative heat transfer is computed by the discrete ordinate (DO) method.

Targeted Combustor and Computational Details

Fig.1 shows the tested sector combustor rig (3/18 sector), which is numerically investigated in this study. The combustor design is RQL (Rich burn, Quick quench, Lean burn) which is a simple design type of low NOx combustor. Fig. 2 shows the computational domain, which corresponds to 1/18 sector of the whole annular combustor. The climbing condition (approximately 85% of maximum engine operating condition), where NOx regulation is critical, is chosen for this study. The investigated two liner designs are summarized in Fig. 3. In CASE-A, a base liner design, namely single wall liners with film cooling holes is adopled. In CASE-B, on the othet hand, double wall liner design with dump cooling flow is adopted in order to move the liner cooling air outlet location from the primary combustion region upstream to the lean combustion region downstream.

The computational domain is divided into about 20 million cells. The internal pressure is 2.1 MPa, and the initial temperatures of the air and fuel droplets were set to those under the engine operating condition. The CPU time

was approximately 200,000 hours (the wallclock time was about 16 days by a parallel computation using 512 cores) for 100,000 steps on the supercomputer of ACCMS, Kyoto University.

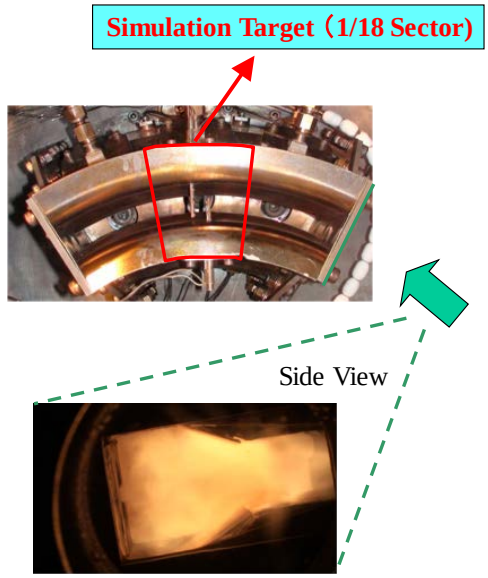

Fig.1 Sector rig combustor

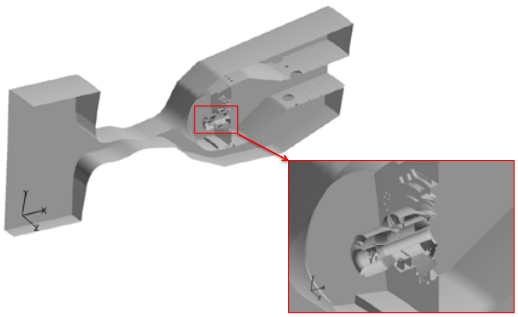

Fig.2 Computational domain

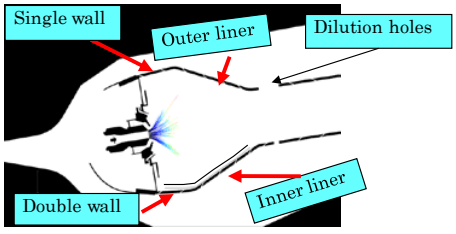

CASES	CASE-A	CASE-B
Outer liner	Single wall	Double wall
Inner liner	Single wall	Double wall

Fig.3 Schematic of wall configuration with simulated cases and conditions

RESULTS AND DISCUSSION

General flow structure

Fig. 4 shows an instantaneous snapshot of iso-surfaces of temperature and fuel sprays swirling with a hollow-cone shape, from which the general turbulent reactive flow feature of spray combustion can be observed.

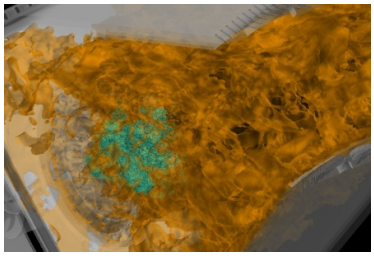

Fig.4 LES results: Snapshot of iso-surfaces of temperature and fuel sprays

Fig. 5 shows the comparisons of time-averaged velocity magnitude distribution for CASE-A and CASE-B. Both shows the general RQL combustor flow field feature. RQL combustor is composed of primary combustion zone, where fuel sprayed with small part of total inlet air with fuel-rich combustion upstream, and lean combustion zone, where fuel-rich primary combustion flow is diluted by large amount of dilution air flow downstream. The difference between the simulated two cases is the flow along the liner-wall in the primary combustion zone. In CASE-A, cooling air is flowing into the primary combustion zone through the single-wall liner and flows along the liner wall. On the other hand, in CASE-B, because the liner wall facing to the high temperature combustion gas is cooled by air flowing in the double-wall liner channel, there is no air flow into the primary combustion zone through the liner and only the dome-cooling air flows along the liner surface.

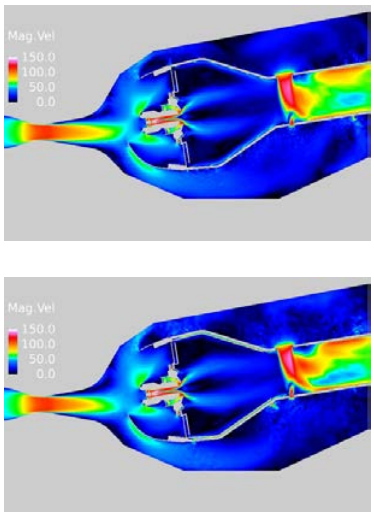

Fig.5 LES results: Averaged velocity magnitude distribution (upper, CASE-A; lower, CASE-B)

Fig. 6 shows the time-averaged O2 mass fraction distribution. There is little O2 left in the primary combustion zone where most of O2 is spent in fuel-rich environment for both cases. However, there is more O2 in the upstream stagnation zone in CASE-B compared with CASE-A. Fig. 7 shows the averaged fuel mass concentration for both cases and it is can be observed that fuel spreads more in this region in CASE-A and there is little fuel going out of the fuel spray cone in CASE-B. From those it can be reasoned that without liner cooling flow in CASE-B the reactive flow field is changed so that smaller amount of fuel is supplied outer upstream away from the spray cone and forms the oxidizer-rich stagnation zone. In other words, the stagnation zone in CASE-A has more efficient fuel-air mixing and reacting flow structure by the liner cooling flow.

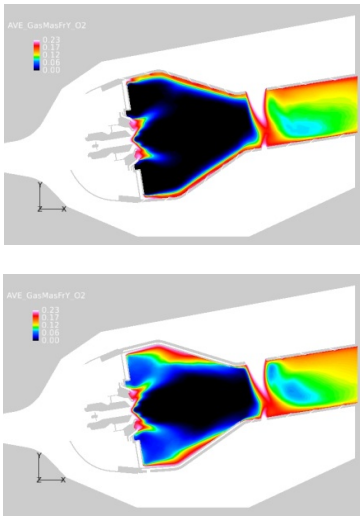

Fig.6 LES results: Averaged O_2 mass fraction distribution (upper, CASE-A; lower, CASE-B)

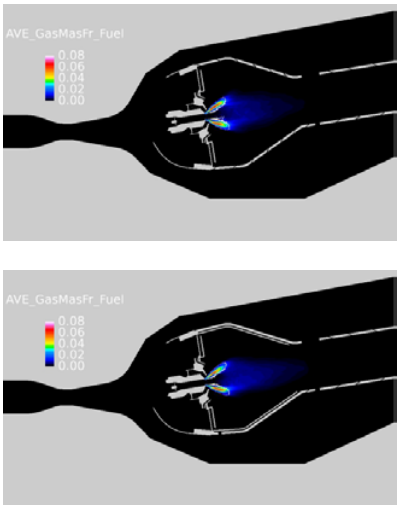

Fig.7 LES results: Averaged fuel mass fraction distribution (upper, CASE-A; lower, CASE-B)

Temperature distribution

Fig. 8 is the predicted instantaneous gas temperature (normalized by combustor inlet temperature) and Fig. 9 is the time-averaged gas temperature distributions for CASE-A and CASE-B respectively. The white dots in the region close to the fuel nozzle in those figures indicate the fuel droplets. Fuel droplets injected from the swirl fuel nozzle are observed to spread outward forming a hollow spray cone and quickly evaporate in the upstream region before the gaseous temperature significantly rises as can be also recognized in Fig. 4.

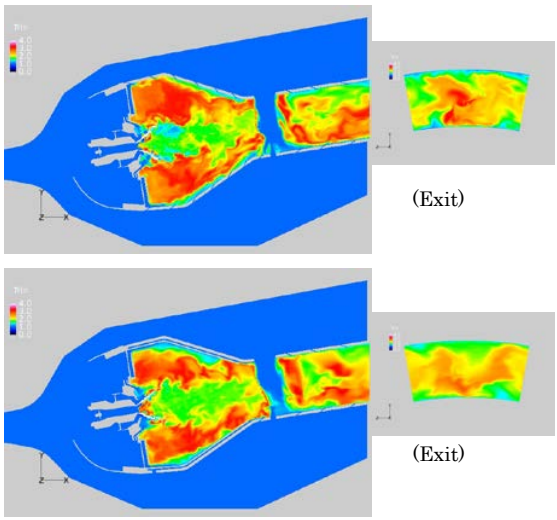

Fig.8 LES results: Instantaneous gas temperature distribution (normalized by inlet temperature, upper, CASE-A; lower, CASE-B)

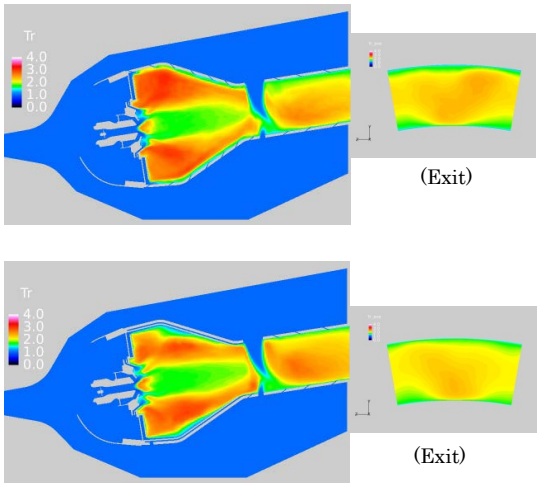

Fig. 9 LES results: Time-averaged gas temperature distribution (normalized by inlet temperature, upper, CASE-A; lower, CASE-B)

The real fuel spray can be observed in Fig. 1 (combustor side view in operation) and the cone shape seems similar to the LES results. A ring-shaped droplet cluster formed by the swirl fuel nozzle breaks and separates into several isolated droplet clusters because of strong fluid shear caused by swirling flow. Compared to CASE-A, CASE-B has overall lower gas temperature in the primary combustion zone. Because this zone is mostly fuel-rich, film cooling air flow from the single wall liner cooling holes in CASE-A forms higher local gas temperature.

Fig. 10 shows the validation of the normalized combustor exit temperature distribution along the radial span (Radial Temperature Distribution Factor; RTDF); which is defined as:

$$RTDF = \frac{T - T_{mean}}{T_{mean} - T_{inlet}} \quad (13)$$

RTDF quantifies the radial temperature variations from its mean planar value. From Fig. 10, LES and experimental results shows fair agreement for both cases but some discrepancy exist especially for CASE-B. LES or CFD in general handles the ideal geometry and boundary conditions but in reality there are some experimental uncertainties. In this case the combustor rig for CASE-B is considered to have some cooling flow unbalance between outer liner and inner liner due to manufacturing tolerance and some mechanical deformation after the series of severe tests, which leads to some deviation from the ideal CFD model geometries.

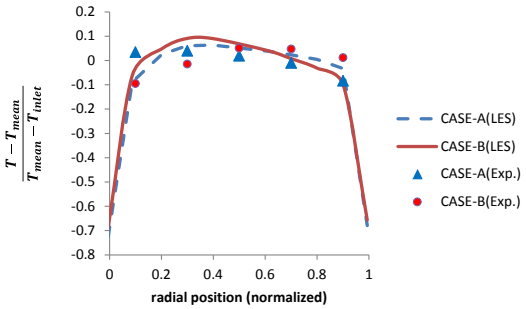

Fig. 10 LES results: Normalized combustor exit temperature distribution along the radial span (RTDF) with experimental data

NO distribution

Fig. 11 shows the time-averaged NO concentration distribution. Compared with the temperature distribution of Fig. 9, it is observed that the higher temperature regions correspond to the high NO region in general. However, there are three major observations contrary to this tendency.

(1) Maximum NO is observed in the lean burn zone close to the combustor exit for both cases although it has lower temperature than primary combustion zone upstream.

(2) More NO is observed for in the stagnation region in the primary combustion zone of CASE-B compared to CASE-A, although CASE-A has higher temperature in this region.

(3) Less NO is observed at the combustor exit especially near the liner wall of CASE-B compared to CASE-A, although the temperature distribution shows little difference between them.

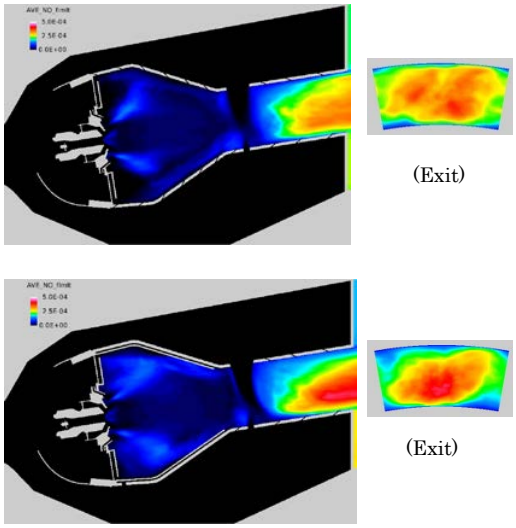

Fig.11 LES results: Time-averaged NO concentration distribution (upper, CASE-A; lower, CASE-B)

NO generation is influenced by three major factors in the combustor internal environment; temperature, residence time, and O2 (or O) mass fraction, if the pressure difference is negligible. For (1), it could be explained that those three major factors are all satisfied in the direction of NO increase at the combustor exit (higher temperature, longer residence time, and enough O2). For (2), Oxygen-rich environment in the stagnation region upstream of CASE-B as shown in Fig. 6 could explain that NO equilibrium is shifted in the direction of NO increase due to excess O2 environment. However, NO decreases rapidly as the flow going downstream along the liner wall in the primary combustion zone of CASE-B, because available O2 also decreases rapidly. On the other hand, O2 is constantly supplied from the single-wall liner cooling holes in CASE-A and NO increased gradually along the liner wall and reach the combustor exit, which could explain (3). In other words, double-wall liner design in CASE-B suppresses the gas temperature increase, NO equilibrium shift due to higher temperature and O2-rich condition near the liner wall, and NO increase at the combustor exit due to longer residence time, by preventing the liner cooling air from mixing with the fuel rich reacting flow in the primary combustion zone.

Fig.12 shows the comparison of NO mass fraction at the combustor exit between the experiments, LES, and RANS (Reynolds-averaged Navier-Stokes) Simulation for

reference. Although RANS results shows about 1/3 NO value of the experimental results, The LES results show NO value close to the experiments. This suggests that present LES is able to quantitatively predict NO emission for the combustor aerodynamic design.

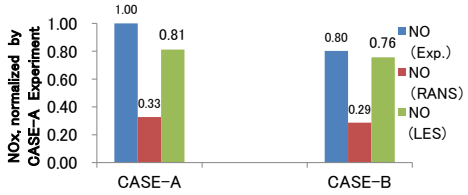

Fig.12 Comparison of NO concentration at combustor exit between LES, RANS and experiments

CONCLUSIONS

In this study, Large-eddy simulation (LES) was applied to a turbulent spray combustion field in a sector combustor for a regional jet aircraft engine under development. The effects of liner-cooling air flow outlet locations (i.e., single/double wall liner designs) on the combustion behaviour and NOx emission were investigated. The main results obtained in this study can be summarized as follows.

(1) The present LES is capable of capturing the general features of the turbulent spray combustion fields in combustors with complex geometries.

(2) The double wall liner design seems desirable for low NOx RQL combustor. This design suppresses NO generation by preventing the liner cooling air from mixing with the fuel rich reacting flow in the primary combustion zone upstream.

ACKNOWLEDGEMENTS

This research was partly supported by the Strategic Programs for Innovative Research (SPIRE) - Field No. 4: Industrial Innovations project of the Ministry of Education, Culture, Sports, Science, and Technology (MEXT).

REFERENCES

Baba, Y., and Kurose, R., 2008, "Analysis and flamelet modeling for spray combustion", *Journal of Fluid Mechanics*, 612, 45-79.

Blanquart, G., Pepiot-Desjardins, P., and Pitsch, H., 2009, "Chemical mechanism for high temperature combustion of engine relevant fuels with emphasis on soot precursors", *Combustion and Flame*, 156, 588-607.

Demirdžić, I., Lilek, Ž., and Perić, M., 1993, "A collocated finite volume method for predicting flows at all speeds", *International Journal of Numerical Methods in Fluids*, 16, 1029-1050.

Fujita, A., Watanabe, H., Kurose, R., and Komori, S., 2013, "Two dimensional direct numerical simulation of spray flames. Part 1: Effects of equivalence ratio, fuel droplet size and radiation, and validity of flamelet model", *Fuel*, 104, 515-525.

Kitano, T., Nakatani, T., Kurose, R., and Komori, S., 2013, "Two dimensional direct numerical simulation of spray flames. Part 2: Effects of ambient pressure and lift, and validity of flamelet model", *Fuel*, 104, 526-535.

Kitano, T., Nishio, J., Kurose, R., and Komori, S., 2014a, "Effects of ambient pressure, gas temperature and combustion reaction on droplet evaporation", *Combustion and Flame*, 161, 551-564.

Kitano, T., Nishio, J,. Kurose, R., and Komori, S., 2014b, "Evaporation and combustion of multicomponent fuel droplets", *Fuel*, 136, 219-225.

Kurose, R., Makino, H., Komori, S., Nakamura, M., Akamatsu, F., and Katsuki, M., 2003, "Effects of outflow from the surface of a sphere on drag, shear lift, and scalar diffusion", *Physics of Fluids*, 15, 2338-2351.

Luo, K., Fan, J., and Cen, K., 2013, "New spray flamelet equations considering evaporation effects in the mixture fraction space", *Fuel*, 103, 1154-1157.

Miller, R. S., and Bellan, J., 1999, "Direct numerical simulation of a confined three-dimensional gas mixing layer with one evaporating hydrocarbon-droplet-laden stream", *Journal of Fluid Mechanics*, 384, 293-338.

Moriai, H., Hayashi, J., Wang, P., Nakatsuka, N., Akamatsu, F., Kurose, R., and Komori, S., 2011, "Optical measurement of spray combustion fields in a sub-scale model for aircraft gas turbine engine combustor", *Journal of. Gas Turbine Society of Japan*, 39, 125-130.

Moriai, H., Kurose, R., Watanabe, H., Yano, Y., Akamatsu, F., and Komori, S., 2013, "Large-eddy simulation of spray combustion in subscale aircraft jet engine combustor -Prediction of Nox and soot concentrations-", *Journal of Engineering for Gas Turbines and Power*, 135, 091503.

Moriai, H., and Miyake, Y., 2008, "Aircraft engine and spray combustion technology", *Combustion Society of Japan*, 50, 225-234.

Nakamura, M., Akamatsu, F., Kurose, R., and Katsuki, M., 2005, "Combustion mechanism of liquid fuel spray in gaseous flame", *Physics of Fluids*, 17, 123301.

Narayanaswamy, K., Blanquart, G., and Pitsch, H., 2010, "A consistent chemical mechanism for oxidation of substituted aromatic species", *Combustion and Flame*, 157, 1879-1898.

Pierce, C. D., and Moin, P., 2004, "Progress-variable approach for large-eddy simulation of non-premixed turbulent combustion", *Journal of Fluid Mechanics*, 504, 73-97.

Pitsch, H., 1998, *A c++ computer program for 0-D combustion and 1-D laminar flame calculation*, RWTH Aachen.

Tachibana, S., Saito, K., Yamamoto, T., Makida, M., Kitano, T., and Kurose, R., 2015, "Experimental and numerical investigation of thermo-acoustic instability in a liquid-fuel aero-engine combustor at elevated pressure: validity of large-eddy simulation of spray combustion", *Combustion and Flame*, doi:10.1016/j.combustflame.2015.03.014.

Watanabe, H., Kurose, R., Hayashi, M., Kitano, T., and Komori, S., 2014, "Effects of ambient pressure and precursors on soot formation in spray flames", *Advanced Powder Technology*, 25, 1376-1387.

Watanabe, H., Kurose, R., Hwang, S.-M., and Akamatsu, F., 2007, "Characteristics of flamelet in spray flames formed in a laminar counterflow", *Combustion and Flame*, 148, 234-248.